European Polymer Journal 109 (2018) 222–228

Contents lists available at ScienceDirect

European Polymer Journal

journal homepage: www.elsevier.com/locate/europolj

Assembly of poly-3-(hexylthiophene) nanocrystals in marginal solvent: The role of PCBM

Marta Da Pian[a], Michele Maggini[a], G. Julius Vancso[b], Valerio Causin[a,*], Edmondo M. Benetti[c,*]

[a] Department of Chemical Science, University of Padova, via Marzolo 1, 35131 Padova, Italy
[b] Materials Science and Technology of Polymers (MTP), University of Twente, Mesa+ Institute for Nanotechnology, 7500 AE Enschede, the Netherlands
[c] Polymer Surfaces Group, Laboratory for Surface Science and Technology, Department of Materials, ETH Zürich, Vladimir-Prelog-Weg 1-5/10, CH-8093 Zurich, Switzerland

ARTICLE INFO

Keywords:
Poly-3-(hexyl thiophene)
Polymer crystallization
Atomic force microscopy
Nanocrystals
X-ray scattering

ABSTRACT

Poly-3-(hexyl thiophene) (P3HT) represents the benchmark semiconducting polymer for the fabrication of organic photovoltaics (OPVs), where it acts as electron donor component in combination with [6,6]-phenyl-C61-butyric acid methyl ester (PCBM), as electron acceptor counterpart. The assembly of P3HT under marginal solvent conditions to form dispersions of fibrillar nanocrystals (NCs) is a particularly attractive method for the subsequent fabrication of highly crystalline films, if compared to depositions involving polymer solutions followed by relatively harsh thermal/solvent treatments, which are often incompatible with sensitive substrates. However, the mechanisms that drive the assembly of P3HT to NCs in marginal solvents are not fully understood, while the effects induced by the presence of PCBM during polymer assembly are still debated. In order to shed light into these processes, we systematically investigated the aggregation/crystallization behaviour of P3HT to NCs under different marginal-solvent conditions and in the presence of different relative contents of PCBM. The starting concentration of P3HT was shown to influence assembly kinetics, the micro-/nano-morphology and the photophysical properties of the formed NCs, as demonstrated by combining atomic force microscopy (AFM) and UV–vis adsorption spectroscopy. Polymer assembly to NCs was also highly dependent on the relative concentration of PCBM, within P3HT:PCBM mixtures typically applied in OPVs. In particular, the combination of UV–vis, AFM and wide-angle X-ray scattering (WAXD) highlighted that PCBM confined the aggregation/crystallization process of P3HT NCs, allowing the formation of extended crystallites, while at high concentrations it hindered the formation of NCs slowing down their assembly.

1. Introduction

Due to its optimal combination of optical and charge-transport properties, poly(3-hexylthiophene) (P3HT) has gained a prominent role as benchmark material for the fabrication of organic photovoltaics (OPVs), field-effect transistors (FETs) and organic light-emitting diodes (OLEDs) [1–5]. In particular, P3HT has been largely employed as electron donating component in the fabrication of OPVs in combination with [6,6]-phenyl-C61-butyric acid methyl ester (PCBM) as electron acceptor, to produce bulk-heterojunction solar cells. In these devices, P3HT and PCBM are thoroughly mixed together usually starting from solutions where the polymer is dissolved, while polymer aggregation and organization are later on induced by solvent evaporation during drop-casting or spin-coating. However, these fabrication processes do not allow the formation of extended crystallites, a necessary pre-requisite to obtain high charge-transport mobilities. Thus, thin films of P3HT require further physical processing, sometimes involving thermal or solvent annealing in order to enhance size and quality of P3HT crystallites [6]. These treatments are often incompatible with sensitive OPV supports such as plastics, therefore practical methods for the direct deposition of highly crystalline P3HT on supports without post-deposition processes, continue to be a challenge [7–9]. Thermal processing of P3HT films can be successfully circumvented by preliminarily assembling polymer nanocrystals (NCs) in solution and subsequently depositing the formed dispersions on the target substrates. The application of P3HT NCs assembled by these procedures presents several advantages over the fabrication of crystalline thin films via polymer melts or solutions. Through the use of solvent-non solvent mixtures or marginal solvents (by the so-called whisker method) [10], highly crystalline P3HT NCs showing extended nanofibrillar morphologies and featuring high hole mobility and large absorption coefficients are obtained [4,11,12]. The formation of NC suspensions enables the fine

* Corresponding authors.
E-mail addresses: valerio.causin@unipd.it (V. Causin), edmondo.benetti@mat.ethz.ch (E.M. Benetti).

https://doi.org/10.1016/j.eurpolymj.2018.09.049
Received 26 April 2018; Received in revised form 19 September 2018; Accepted 24 September 2018
Available online 25 September 2018

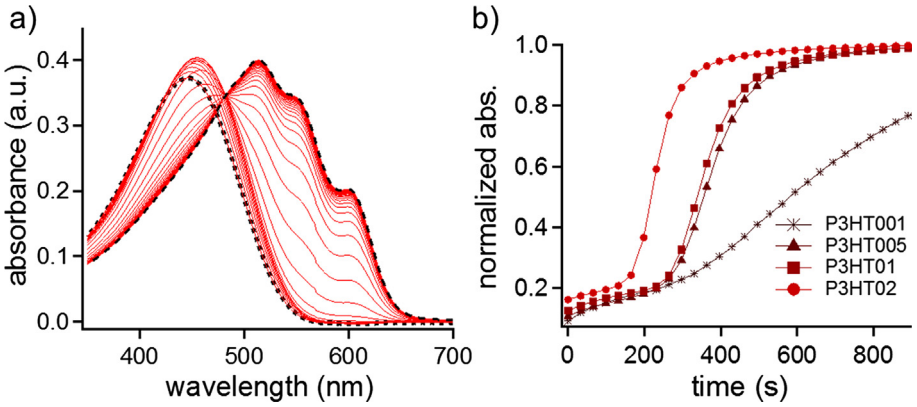

Fig. 1. (a) UV–vis absorption spectra of P3HT01 suspension recorded every 30 s upon cooling from 95 °C (black dotted trace) to RT (black dashed trace); (b) kinetics of P3HT NCs formation from different starting polymer concentrations obtained by plotting the sum of 0–0, 0–1 and 0–2 band intensities, normalized at the isosbestic point, as a function of time (from 95 °C, t = 0 s to RT, t = 900 s).

control over the nanomorphology of the subsequently deposited films by the simple tuning of the crystallization parameters in the feed solution. The size of P3HT NCs assembled by whisker method matches the typical exciton wavelengths, while their intrinsic morphology permits a very large donor/acceptor interfacial area for efficient exciton dissociation. Finally, the fibre-like shape of NCs assembled by these methods enables the formation of a continuous and percolated network, which can readily become co-continuous when mixed with PCBM.

Hence, P3HT-PCBM mixtures already presenting well dispersed phases can be obtained in one-pot preparations onto a variety of supports, including flexible (polymeric) substrates [10,13–17].

Despite the verasatility of these methods, a commonly encountered phenomenon in the manipulation of P3HT NCs is the intrinsic tendency by the NCs to strongly interact in marginal solvent conditions due to van der Waals forces. This behaviour limited the processability of their dispersions especially at high polymer concentrations, when the interactions between NCs induce the formation of extended networks causing macroscopic aggregation and gelation [13,18].

In order to clarify the parameters determining the formation of P3HT NCs, we systematically investigated their assembly using anisole as marginal solvent, and varying the starting polymer concentration. We specifically focused on the aggregation kinetics, the photophysical properties of the formed aggregates, studied by UV–vis absorption spectroscopy, and their micro-/nanomorphology, investigated by atomic force microscopy (AFM). Particular attention was dedicated to the main driving forces involved in the formation of NC dispersions i.e. crystallization-driven assembly to form NCs and van der Waals interactions between already assembled NCs, which influence the morphology of larger micro-aggregates of NCs. In addition, we investigated the formation of NCs in the presence of PCBM dissolved in anisole during polymer aggregation, applying relative concentrations of the two components similar to those used to fabricate OPVs. The presence of PCBM was demonstrated to influence the aggregation kinetics and the formation of P3HT NCs, partially hindering the assembly of extended crystallites and slowing down their formation.

2. Experimental section

Regioregular P3HT was synthesized by Grignard metathesis polymerization with the method introduced by McCullough et al. [19] P3HT was characterized by NMR spectroscopy and gel permeation chromatography (GPC) using a Phenomenex Phenogel 5 MXM 300 mm × 7.8 mm 5 μm particle size 5–500 K and chloroform as eluent. The P3HT sample synthesized for this study was characterized by 97% of regioregularity, a molecular weight of 15.300 Da and a polydispersity index (PDI) of 1.3. AFM micrographs of P3HT NCs (dispersed on freshly cleaned silicon substrates) were recorded by tapping-mode AFM using a Nanoscope Dimension (Veeco Digital Instruments, Santa Barbara CA, USA).

WAXD reflection patterns were recorded on P3HT NCs suspensions, drop-casted on silicon oxide wafers. A Philips X'Pert PRO diffractometer equipped with a graphite monochromator on the diffracted beam (Cu Ka radiation) was employed. The angular range for the measurements in the reflection geometry was 1.5–30 2θ.

UV–Vis absorption spectra were recorded on a Varian Cary 5000 double-beam UV–Vis-NIR spectrophotometer and baseline corrected.

3. Results and discussion

The formation of P3HT NCs from 0.02, 0.01, 0.005 and 0.001% w/w mixtures in anisole (samples named P3HT02, P3HT01, P3HT005 and P3HT001, respectively) was comparatively investigated. The different mixtures were first heated at 95 °C obtaining transparent solutions that were, later on, progressively cooled at room temperature allowing the formation of NC suspensions. The aggregation and growth of the NCs during cooling from 95 °C to room temperature was followed in situ by UV–Vis spectroscopy. Fig. 1**a** shows representative UV–Vis profiles obtained for sample P3HT01. At 95 °C (dotted profile) a symmetrical band, centred at 450 nm, develops from the intra-chain electronic transition of P3HT, which is completely soluble at this temperature and adopts a coil-like conformation (similar profiles could be registered for all the concentrations tested, as reported in Fig. S1 in the Supporting Information) [22].

The decrease of the temperature caused a transition of the polymer from coils to rods [20,21], with a concurrent chain planarization and increment of conjugation length that produced a red shift of the main absorption peak. The appearance of the π-π* bands at 525, 550, and 610 nm (corresponding to 0–2, 0–1 and 0–0 transitions, respectively) following further cooling was caused by the aggregation of P3HT rods into NCs. The presence of a clear isosbestic point at 475 nm indicated that the transition from dissolved into aggregated macromolecules occurred directly, without intermediate states [13]. The absorption intensities of the π-π* transitions, normalized at the isosbestic point, were plotted from time 0 s (95 °C, traced as dotted line in Fig. 1a) to 900 s (room temperature, traced as a dashed profile in Fig. 1a), providing the kinetics of polymer assembly into NCs. The rate profiles for the different P3HT concentrations are reported in Fig. 1**b** and clearly showed a characteristic sigmoid shape which became steeper as the polymer concentration increased. For P3HT01, P3HT02 and P3HT005, the formation of ordered aggregates seemed to reach a plateau after 400–600 s. Interestingly, in the case of the most diluted P3HT001 sample, this steady crystallization state was reached at much longer times at ambient temperature (around 1400 s, data points reported in Fig. S2 in the ESI). The observed, increment in aggregation rate with increasing polymer concentration was also accompanied by a simultaneous decrease in the induction time before the assembly of NCs was triggered, i.e. less than 200 s for P3HT02, ~300 s for P3HT01 and P3HT005 and ~350 s for the most diluted P3HT001.

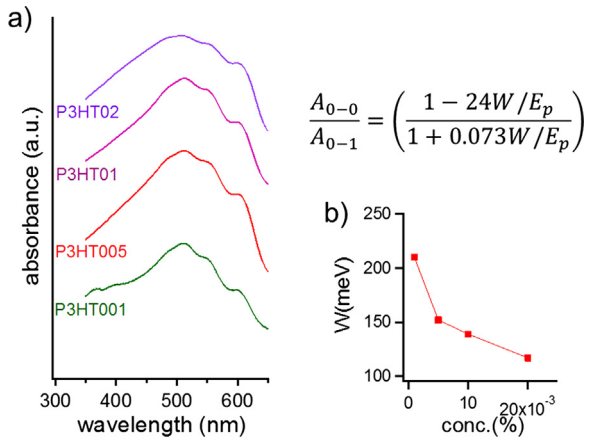

Fig. 2. (a) UV–vis absorption profiles of P3HT NCs suspensions aged for 24 h and obtained from different P3HT starting concentrations; (b) values of the exciton bandwidth W calculated from the relative absorbance of the 0–0 and 0–1 bands obtained from the profiles reported in (a) using the equation reported in the inset of the Figure proposed by Spano et al. [21,23].

A higher concentration of soluble P3HT coils at high temperatures thus turned into a faster and immediate assembly into NCs once the temperature was lowered.

Since a slow crystallization kinetics is usually associated to extended crystalline domains, UV–vis, AFM and optical microscopy (OM) were performed in order to investigate whether morphology and photophysics of NCs varied with the starting polymer concentration.

The absorption characteristics of P3HT NCs were recorded by UV–vis on NCs suspensions aged for 24 h (Fig. 2a). All spectra displayed a structured profile with discrete bands originating from π-π* transitions centred at 525, 550, and 610 nm [13,17]. Relevantly, the relative intensity of these bands showed just a slight variation if the NC suspensions were aged for further ten days after the assembly (Supporting Information).

A deeper insight into the properties of the NCs formed from different starting concentrations of P3HT was provided by a detailed analysis of the π-π* bands in the corresponding absorption spectra. Comparing the spectra reported in Fig. 2a, the ratio between the absorbance of 0–0 and 0–1 bands uniformly decreased with increasing P3HT feed concentration. According to a model introduced by Spano [21,23], the relative intensities of the 0–0 and 0–1 bands are related to the free exciton bandwidth W of the NCs as stated in the equation reported in Fig. 2b, where $A_{0\text{-}0}$ and $A_{0\text{-}1}$ are the absorbance values of the bands at 610 nm and at 550 nm, respectively, and E_p is the phonon energy of the main oscillator mode coupled to the electronic transition, which was reported to be equal to 0.179 eV [21,24]. Fig. 2b shows that W decreased with the feed concentration of P3HT. Since, the excitonic bandwidth W is related to the resonant Coulomb (excitonic) coupling (J) through $W = 4|J|$, the values of J for the P3HT NC suspensions prepared in this work ranged from ~50 eV, for P3HT001, to ~30 eV, in the case of the most concentrated P3HT02.

The excitonic bandwidth represents a particularly interesting parameter because it is related to the conjugation length [20,23], with a J value of 30 eV resulting equal to 20–30 monomer units [21,24]. Moreover, since J (and consequently W) decreases as the conjugation length increases [21,24], the data shown in Fig. 2b implied that, somewhat counter-intuitively, a slower process of NC formation was not associated to a higher degree of order. Thus UV–vis analysis of P3HT NCs indicated that increasing the concentration of the starting P3HT solution induced the formation of NCs with higher conjugation length and fewer defects.

In order to investigate the micro- and nanomorphology of the different P3HT NCs suspensions, both OM and AFM were performed on films obtained by spin-coating P3HT NC suspensions on silicon oxide substrates.

In all the different samples studied, P3HT NCs showed a tendency to form larger structures made of extended aggregates of NCs, held together by van der Waals interactions [21]. The morphological characteristics of these micro-aggregates were shown to be concentration dependent. As depicted in Fig. 3, for both concentrated (as shown for P3HT01) and diluted (P3HT001) suspensions, large micro-aggregates of NCs with typical dimensions between 50 and 100 μm were formed following 24 h of aging (Fig. 3b and d). These aggregates were formed by the assembly of single NCs, as shown in Fig. 3a and c for P3HT01 and P3HT001, respectively. Additionally, the micro-aggregates showed a closer packing and a higher density for higher P3HT concentrations (Fig. 3b for P3HT01) if compared to more diluted P3HT/anisole samples (P3HT001 in Fig. 3d). It was found that this behaviour depended on the incubation time. Smaller and dispersed bundles of P3HT NCs, obtained at low P3HT starting concentrations, progressively tended to organize into larger structures with the increase of the incubation time in anisole. Fig. 3a and c illustrates how, just after formation, P3HT NCs assembled from a 0.001% solution were singly dispersed and invisible by OM, while few small aggregates became detectable by OM in suspensions aged for 24 h.

At higher concentrations, a more extensive bundling of the NCs was observed upon cooling the solution to room temperature and this was accompanied by the formation of NCs micro-aggregates that increased their size with the aging time.

Further AFM analysis revealed the inner structure of the P3HT NC aggregates. Fig. 4 shows that P3HT01 (height micrographs in Fig. 4a

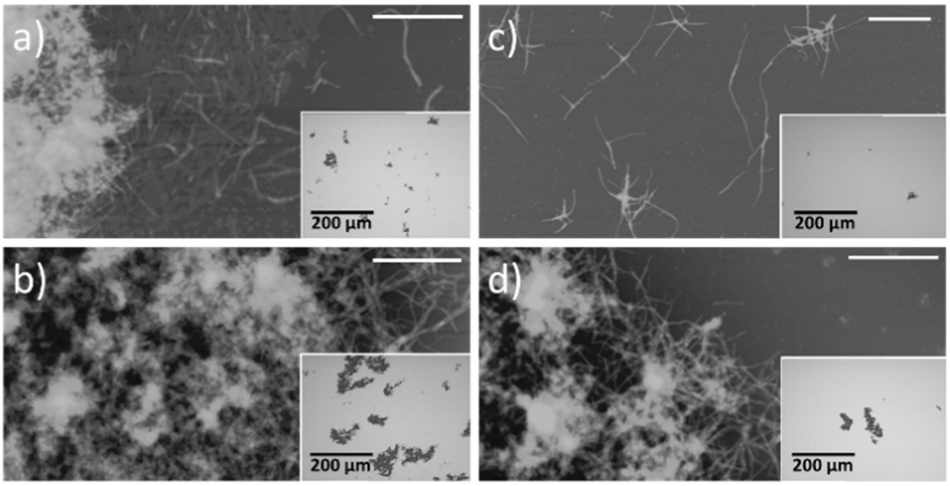

Fig. 3. AFM and optical microscope images (in the insets) depicting the P3HT NCs' assemblies right after aggregation (a and c) and after 24 h aging (b and d) for two different feed concentrations of P3HT, namely 0.01% (a and b, named as P3HT01) and 0.001% in anisole (c and d, named P3HT001). The white scale bar corresponds to 1.5 μm. The corresponding OM micrographs are shown in the insets.

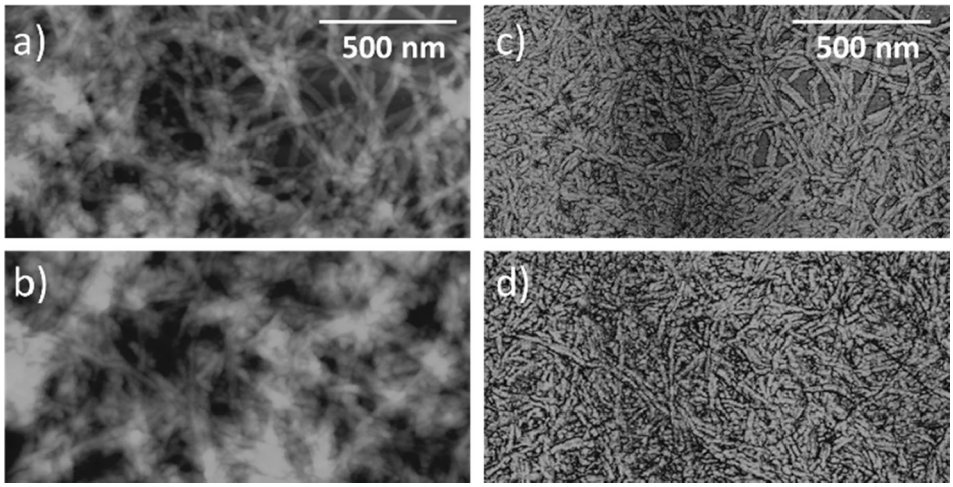

Fig. 4. AFM micrographs depicting the P3HT NCs assemblies after 24 h aging for P3HT01 ((a) heigh and (c) phase micrograph) and P3HT02 ((b) heigh and (d) phase micrograph).

and corresponding phase images in Fig. 4c) and P3HT02 (height and phase micrographs in Fig. 4b and d, respectively) are constituted by extended assemblies of P3HT NCs. Each NC presented typical width of 5–10 nm and lengths ranging from few hundred nm to several microns. In particular a slightly denser organization of NCs was recognized for P3HT02 if compared to P3HT01, due to the tighter packing of fibres obtained at higher P3HT starting concentrations.

The formation of P3HT NCs under conditions similar to those applied for formulating OPV mixtures was subsequently investigated. Namely, P3HT aggregation from anisole dispersions and the morphological characteristics of the resulting NCs were investigated in the presence of increasing amounts of PCBM.

Different P3HT:PCBM mixtures were prepared, namely 1:1, 1:3 and 1:5 (P3HT:PCBM weight ratios), and the kinetics of NCs' formation were followed for each mixture by UV–vis spectroscopy. A constant feed concentration of 0.025% w/w P3HT was chosen due to the lowest *W* value obtained for the derived suspensions (90 meV). In addition, this particular concentration produced NC networks displaying highly percolated morphology and densely packed crystalline aggregates.

As reported in Fig. 5, similarly to pure P3HT solutions, the absorption spectra of P3HT:PCBM mixtures evolved from a single peak located at 450 nm (black dotted profile in each spectrum reported in Fig. 5) which corresponded to dissolved P3HT at 95 °C, to more structured patterns, with the π-π* bands appearing at 525, 550, and 610 nm due to the formation of P3HT NCs. At shorter wavelengths, the presence of PCBM induced an increment in absorbance, the intensity of the characteristic band centred at 335 nm increasing upon rising the relative PCBM concentration [25]. Previous reports focusing on P3HT:PCBM films reported that the addition of PCBM caused a marked blue shift of P3HT π-π* bands. This was ascribed to the twisting of the polymer backbones, the loss of the degree of order of the P3HT framework and, concurrently, a decrease in hole mobility [25,26]. In this study no shift was observed in the position of the π-π* bands for P3HT-PCBM suspensions. This result suggested that the inner structure of P3HT crystallites produced by the whisker method was not affected by the addition of PCBM.

However, the values of *W* for the three different mixtures were found slightly higher if compared to those recorded for the corresponding «pure» P3HT NCs. Namely, *W* was 119, 125 and 120 meV for 1:1, 1:3 and 1:5 P3HT:PCBM mixtures, respectively. Since a higher *W* is associated to a shorter conjugation length, it can be concluded that the conformation of the polymer chains in the NCs assembled in the presence of PCBM was slightly more disordered compared to the case of crystallites assembled from solutions containing just polymer.

The effect of PCBM on the assembly kinetics of P3HT NCs was monitored by recording the normalized absorbance of π-π* bands from 95 °C to ambient temperature. As shown in Fig. 6a, in all cases the presence of PCBM slowed down the assembly of P3HT chains to NCs. Moreover, in the presence of PCBM, the induction time before NCs formation was longer than that recorded for pure P3HT, reflecting an hindrance in the nucleation process [27].

Further insight into the formation of NCs in the different mixtures was provided by analyzing the assembly kinetics according to the Avrami theory (Fig. 6b) [28–30]. The construction of the resulting plots did not take into consideration the points in the short time regions since logarithmic plotting tended to overestimate small errors in the assessment of the initial time of crystallization [31].

The results, reported in Table 1, provided represents the kinetic

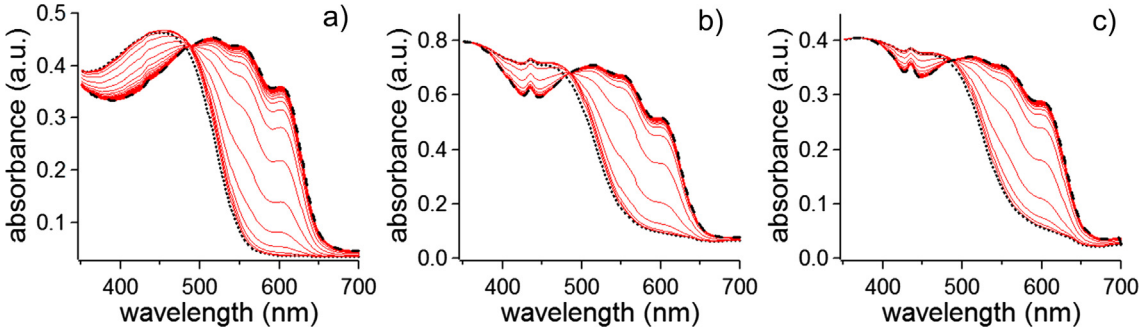

Fig. 5. UV–vis absorption spectra of P3HT:PCBM suspensions recorded upon cooling from 95 °C (black dotted traces) to RT (black dashed traces) for (a) P3HT:PCBM 1:1, (b) P3HT:PCBM 1:3 and (c) P3HT:PCBM 1:5 mixtures.

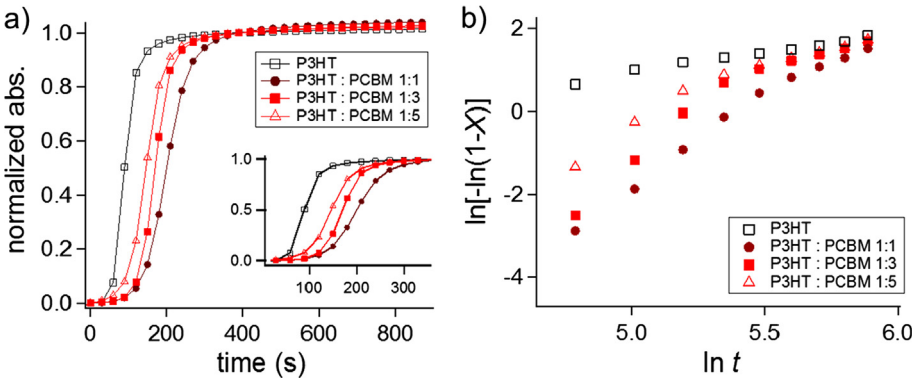

Fig. 6. (a) Rate profiles for the NCs formation in P3HT:PCBM/anisole solutions containing a starting P3HT concentration of 0.025% and different relative amounts of PCBM. The kinetic plots were obtained from the sum of the relative absorbance of π-π* bands normalized at the isosbestic points as a function of time (from 95 °C, t = 0 s to RT, t = 900 s). (b) Avrami plots obtained from the curves reported in Figure (a).

Table 1
Avrami parameters for the formation of NCs in P3HT:PCBM/anisole mixtures.

Sample	ln *K*	*n*
P3HT	−4.0	1.0
P3HT:PCBM 1:1	−13.8	2.6
P3HT:PCBM 1:3	−8.8	1.8
P3HT:PCBM 1:5	−8.1	1.7

constant for NC formation (*lnK*), and the parameter *n*, which is related to the mechanism of nucleation and growth [28–30].

As expected, the value of *K* for NCs assembled in the absence of PCBM resulted much larger than the corresponding values obtained for PCBM:P3HT mixtures. The minimum value of *lnK* was found for the sample containing equal amounts of P3HT and PCBM. When the concentration of PCBM was further raised, *K* increased, although it remained lower than the value of the constant recorded for pure P3HT. Marked shifts in the kinetic constant were also accompained by variations in the values of *n*, which reflected a modification of the crystallization process for P3HT NCs induced by the presence of PCBM. Our results seemed to contrast those of Jeng and co-workers, where PCBM was reported to interfere with the nucleation rate of P3HT lamellae, but not on their growth mechanism [31]. However, these authors concentrated on P3HT:PCBM mixtures spin-coated from chlorobenzene solutions, whereas in this work the formation of P3HT NCs was monitored in marginal solvent conditions. The strong interplay between PCBM and P3HT during the crystallization process, evidenced by the Avrami data, was not unexpected, since several reports confirmed that these two materials are highly miscible, with interdiffusion coefficients larger than 10^{-11} $cm^2 s^{-1}$ and an interaction parameter of about 0.4 [6,32–34].

In order to investigate the quality of P3HT NCs produced in the presence of PCBM we recorded WAXD profiles for all P3HT:PCBM mixtures drop-casted on silicon oxide surfaces (Fig. 7a). The strong signal at 5.4°2θ (1 0 0) was associated to the side-by-side arrangement of the main chains [35,36]. Second- and third-order reflections (2 0 0) and (3 0 0) were related to a higher degree of space filling and with a more significant interdigitation of the alkyl side-chains [13,35].

The qualitative appearance of the WAXD patterns reported in Fig. 7a changed significantly as a function of PCBM content. Pure P3HT, 1:1 and 1:3 mixtures displayed diffraction patterns with relatively weak amorphous halos located at about 20° 2θ, indicating the formation of highly crystalline material [37]. In contrast, an increase in the relative PCBM content to 1:5 determined an increment in intensity of the amorphous halo with a concurrent weakening of the crystalline peaks of P3HT, with (2 0 0) and (3 0 0) reflections resulting barely detectable [38,39]. A further information that could be inferred from the WAXD patterns was the absence of (0 1 0) diffraction signals at about 23.4° 2θ for any of the samples studied. This reflection is commonly originated by the stacking of the layers, formed by the chains arranged side-by-side. The absence of this peak was thus indicating that P3HT layers in these drop-casted NCs films were arranged edge-on, as earlier reported [7,38,39].

Hole mobility was previously found directly dependent on the degree of π-π stacking and chain ordering [15]. Thus, quantitative assessment of the degree of order within the planes formed by the main chains (arranged side-by-side and with their interdigitated hexyl gorups) could be obtained by measuring the relative intensity of the

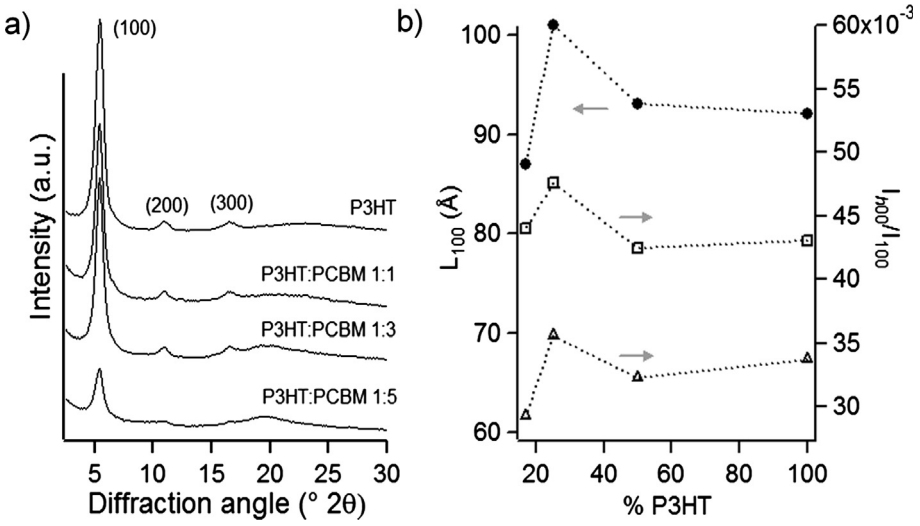

Fig. 7. Diffraction patterns of the samples containing different amounts of P3HT (a) and crystallite size and I_{h00}/I_{100} ratios calculated from the WAXD patterns (b).

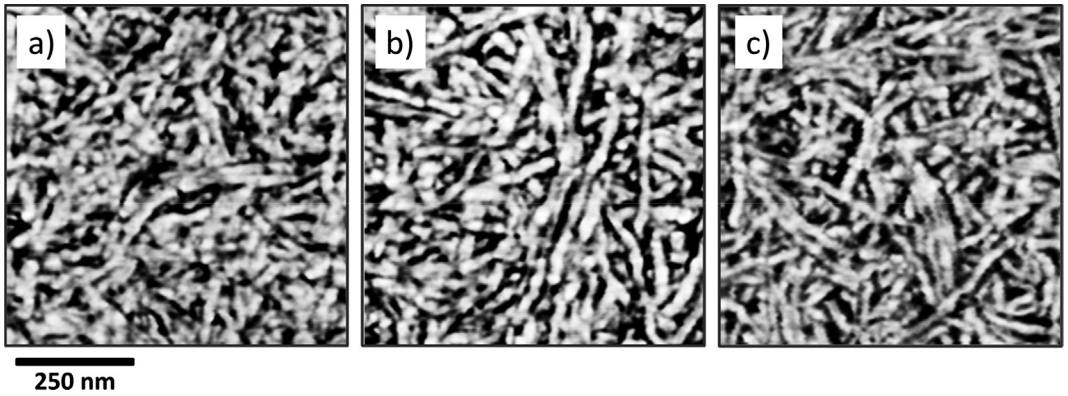

Fig. 8. AFM phase micrographs of P3HT NCs:PCBM mixtures obtained from (a) P3HT:PCBM 1:1, (b) P3HT:PCBM 1:3 and (c) P3HT:PCBM 1:5 relative concentrations (w:w).

higher order signals with respect to the (1 0 0) reflection. Fig. 7**b** shows the values of I_{200}/I_{100} and of I_{300}/I_{100} (where I_{h00} is the intensity of the h00 peak plotted as a function of P3HT relative concentration in the mixtures). As can be seen, this ratio showed a maximum for P3HT:PCBM 1:3 mixture which corresponded to a PCBM weight content of 75%. The same trend was also displayed by the crystallite size (Fig. 7b) which was estimated on the basis of the full width at half maximum (β_0) of the (1 0 0) peak, by the Scherrer equation: [40]

$$L_{100} = 0.91\lambda/\beta_0 cos\theta$$

where L_{100} represents the crystallite thickness in the direction perpendicular to the crystallographic plane identified by Miller indices (1 0 0), λ is the wavelength of the X-radiation and θ the diffraction angle. The obtained values of L_{100} (85–100 Å) resulted in good agreement with the data reported by other authors [7,37,39].

This parameter is of considerable importance because it was suggested that, all other morphological parameters being equal, larger P3HT crystallites produced a more efficient charge transport [41].

The relative size of P3HT NCs that formed in different P3HT:PCBM mixtures could be also confirmed by AFM, performed on the same drop-casted films used for the WAXD characterization. As reported in Fig. 8 NCs organizations in 1:3 P3HT:PCBM showed thicker and more elongated morphologies compared to 1:1 and 1:5 mixtures.

Hence, these results indicated that dispersions of P3HT:PCBM 1:3 generated the largest crystalline P3HT domains among the different mixtures tested, in agreement with the optimum relative concentration of these two components for OPVs fabrication, previously reported by DeLongchamp and co-workers [42].

The effect of PCBM on P3HT assembly to NCs could be summarized into two different phenomena. On the one hand, PCBM slowed down P3HT aggregation/crystallization in a marginal solvent, inducing the presence of defects within the formed NCs. On the other hand an optimum P3HT:PCBM relative concentration triggered the formation of larger crystallites also compared to the pure P3HT solutions by confining the aggregation/crystallization process [38,39,42].

In line with these findings, Jenget al. previously observed that the degree of order of P3HT crystallites derived from an interplay between phase separation of P3HT/PCBM and crystallization of P3HT [27]. Specifically, in P3HT:PCBM systems the polymer seemed rapidly crystallizing while PCBM diffused between the crystallized P3HT domains [6].

4. Conclusion

In this work, we investigated the assembly process of P3HT NCs using anisole as marginal solvent and varying P3HT solution parameters. A steady acceleration of P3HT aggregation/crystallization with starting P3HT solution concentration was found. Differently from other polymers, though, increasing P3HT concentrations triggered the formation of NCs displaying higher order and longer conjugation lengths, as evidenced by UV–vis absorption spectroscopy. The nano-/micro-morphology of NCs were also influenced by the starting concentration of P3HT. Namely, NCs interacting by van der Waals forces tended to aggregate forming micro-aggregates in the dispersions. These superstructures were readily obtained for P3HT concentrations ≥0.01%, while NC dispersions obtained from P3HT concentrations ≤0.001% required slow aging for the formation of micro-aggregates. Thus two main forces determined the aggregation of NCs and the morphological characteristics of the dispersions obtained by *whisker* method: assembly/crystallization, which governed the organization of P3HT rods into NCs, and van der Waals forces, which determined the interaction between already formed NCs.

The presence of PCBM in P3HT:PCBM mixtures was further shown to decrease the rate of assembly/crystallization, while inducing the presence of defects in NCs if compared to their pure P3HT counterparts. Specifically, PCBM had a double, concentration-dependent role in the aggregation/crystallization process of P3HT in marginal solvent. It confined the assembly of P3HT into NCs and induced the formation of extended aggregates while it also induced the formation of defects in P3HT NCs.

Thus, this study highlights that an optimal condition for preparation of OPVs exploiting P3HT NCs prepared through the *whisker* method is yet to come, however, the tendency to self-aggregate and auto-assemble to yield NCs is best exploited if P3HT crystallization is carried out quickly. In fact, the lowest *W* values were obtained with the fastest crystallizing dispersions.

Acknowledgment

Financial support for this work is gratefully acknowledged from the University of Padova through HELIOS (grant STPD08RCX5) and Regione del Veneto (SMUPR n. 4148, Polo di Ricerca nel settore fotovoltaico). E.M.B. wishes to thank the University of Padova and the Mesa + Institute for Nanotechnology for financial support.

Appendix A. Supplementary material

Supplementary data to this article can be found online at https://doi.org/10.1016/j.eurpolymj.2018.09.049.

References

[1] M.R. Andersson, O. Thomas, W. Mammo, M. Svensson, M. Theander, O. Inganas, J. Mater. Chem. 9 (1999) 1933–1940.
[2] J. Pei, W.L. Yu, W. Huang, A.J. Heeger, Macromolecules 33 (2000) 2462–2471.
[3] J.F. Chang, B.Q. Sun, D.W. Breiby, M.M. Nielsen, T.I. Solling, M. Giles, I. McCulloch, H. Sirringhaus, Chem. Mater. 16 (2004) 4772–4776.

[4] M. Chang, J. Lee, P. Chu, D. Choi, B. Park, E. Reichmanis, ACS Appl. Mater. Interfaces 6 (2014) 21541–21549.
[5] C. Liu, K. Wang, X. Gong, A.J. Heeger, Chem. Soc. Rev. 45 (2016) 4825–4846.
[6] F. Liu, Y. Gu, J.W. Jung, W.H. Jo, T.P. Russell, J. Polym. Sci. Polym. Phys. 50 (2012) 1018–1044.
[7] M. Brinkmann, P. Rannou, Macromolecules 42 (2009) 1125–1130.
[8] N. Seidler, G.M. Lazzerini, G. Destri, G. Marletta, F. Cacialli, J. Mater. Chem. C 1 (2013) 7748–7757.
[9] J.Y. Na, M. Kim, Y.D. Park, J. Phys. Chem. C 121 (2017) 13930–13937.
[10] J.T. Chen, C.S. Hsu, Polym. Chem. 2 (2011) 2707–2722.
[11] H. Xin, G. Ren, F.S. Kim, S.A. Jenekhe, Chem. Mater. 20 (2008) 6199–6207.
[12] J.S. Kim, J.H. Lee, J.H. Park, C. Shim, M. Sim, K. Cho, Adv. Funct. Mater. 21 (2011) 480–486.
[13] S. Berson, R. De Bettignies, S. Bailly, S. Guillerez, Adv. Funct. Mater. 17 (2007) 1377–1384.
[14] J.H. Kim, J.H. Park, J.H. Lee, J.S. Kim, M. Sim, C. Shim, K. Cho, J. Mater. Chem. 20 (2010) 7398–7405.
[15] Y. Li, G. Xu, C. Cui, Y. Li, Adv. Energy Mater. (2017) 1701791.
[16] H. Xin, F.S. Kim, S.A. Jenekhe, J. Am. Chem. Soc. 130 (2008) 5424–5425.
[17] E.M. Benetti, V. Causin, M. Maggini, Adv. Mater. 24 (2012) 5636–5641.
[18] N.S. Güldal, T. Kassar, M. Berlinghof, T. Ameri, A. Osvet, R. Pacios, G.L. Destri, T. Unruh, C.J. Brabec, J. Mater. Chem. C 4 (2016) 2178–2186.
[19] R.S. Loewe, S.M. Khersonsky, R.D. McCullough, Adv. Mater. 11 (1999) 250–253.
[20] C.A. Sandstedt, R.D. Rieke, C.J. Eckhardt, Chem. Mater. 7 (1995) 1057–1059.
[21] J. Clark, C. Silva, R.H. Friend, F.C. Spano, Phys. Rev. Lett. 98 (2007) 206406.
[22] S. Malik, T. Jana, A.K. Nandi, Macromolecules 34 (2001) 275–282.
[23] F.C. Spano, J. Chem. Phys. 122 (2005) 234701.
[24] P.J. Brown, S. Thomas, A. Kohler, J.S. Wilson, J.S. Kim, C.M. Ramsdale, H. Sirringhaus, R.H. Friend, Phys. Rev. B 67 (2003) 064203.
[25] V.D. Mihailetchi, H.X. Xie, B. de Boer, L.J.A. Koster, P.W.M. Blom, Adv. Funct. Mater. 16 (2006) 699–708.
[26] V. Shrotriya, J. Ouyang, R.J. Tseng, G. Li, Y. Yang, Chem. Phys. Lett. 411 (2005) 138–143.
[27] W.R. Wu, U.S. Jeng, C.J. Su, K.H. Wei, M.S. Su, M.Y. Chiu, C.Y. Chen, W.B. Su, C.H. Su, A.C. Su, ACS Nano 5 (2011) 6233–6243.
[28] M. Avrami, J. Chem. Phys. 9 (1941) 177–184.
[29] M. Avrami, J. Chem. Phys. 8 (1940) 212–224.
[30] M. Avrami, J. Chem. Phys. 7 (1939) 1103–1112.
[31] Y. Seo, J. Kim, K.U. Kim, Y.C. Kim, Polymer 41 (2000) 2639–2646.
[32] G.A. Berriman, N.P. Holmes, J.L. Holdsworth, X. Zhou, W.J. Belcher, P.C. Dastoor, Org. Electron. 30 (2016) 12–17.
[33] B. Watts, W.J. Belcher, L. Thomsen, H. Ade, P.C. Dastoor, Macromolecules 42 (2009) 8392–8397.
[34] B.A. Collins, E. Gann, L. Guignard, X. He, C.R. McNeill, H. Ade, J. Phys. Chem. Lett. 1 (2010) 3160–3166.
[35] S. Chen, J. Ni, Macromolecules 25 (1992) 6081–6089.
[36] V. Causin, C. Marega, A. Marigo, L. Valentini, J.M. Kenny, Macromolecules 38 (2005) 409–415.
[37] W.D. Oosterbaan, V. Vridts, S. Berson, S. Guillerez, O. Douhéret, B. Ruttens, J. D'Haen, P. Adriaensens, J. Manca, L. Lutsen, D. Vanderzande, J. Mater. Chem. 19 (2009) 5424–5435.
[38] S. Lilliu, T. Agostinelli, E. Pires, M. Hampton, J. Nelson, J.E. MacDonald, Macromolecules 44 (2011) 2725–2734.
[39] Y. Kim, J. Nelson, J.R. Durrant, D.D.C. Bradley, K. Heo, J. Park, H. Kim, I. McCulloch, M. Heeney, M. Ree, C.S. Ha, Soft Matter 3 (2007) 117–121.
[40] H.P. Klug, L.E. Alexander, X-ray Diffraction Procedures, Wiley, New York, 1974.
[41] J. Rivnay, S.C.B. Mannsfeld, C.E. Miller, A. Salleo, M.F. Toney, Chem. Rev. 112 (2012) 5488–5519.
[42] M.J. Sobkowicz, R.L. Jones, R.J. Kline, D.M. DeLongchamp, Macromolecules 45 (2012) 1046–1055.